Research Square

Preprints are preliminary reports that have not undergone peer review.
They should not be considered conclusive, used to inform clinical practice,
or referenced by the media as validated information.

The α2A-adrenergic receptor on Tfh cells amplifies allergic airway inflammation via Akt signaling

Xiao Su

xsu@ips.ac.cn

Shanghai Institute of Materia Medica https://orcid.org/0000-0002-8692-8365

Gelei Lan

Ruijin Hospital, Shanghai Jiao Tong University School of Medicine, Shanghai, China

Juan Du

Jie Chen

Shitao Xie

Xiaoyun Lai

Yahui Liu

Chunrong Huang

Xueqing Du

Yidan Sun

Guochao Shi

Article

Keywords: Asthma, α2AR (α2A adrenergic receptor), Tfh cells, germinal center B cells, AKT signaling, neuroimmune regulation

Posted Date: November 14th, 2025

DOI: https://doi.org/10.21203/rs.3.rs-7932656/v1

License: This work is licensed under a Creative Commons Attribution 4.0 International License.
Read Full License

Additional Declarations: There is **NO** Competing Interest.

Version of Record: A version of this preprint was published at Communications Biology on July 13th, 2026. See the published version at https://doi.org/10.1038/s42003-026-10670-6.

Abstract

Bronchial asthma is a prevalent chronic inflammatory disease characterized by aberrant immune regulation. While β2-adrenergic signaling has been extensively studied in asthma, the role of other adrenergic receptors remains unclear. Here, we identify α2A-adrenergic receptor (α2AR, coded by *Adra2a*) as a key modulator of allergic airway inflammation. Transcriptomic analysis of house dust mite (HDM)-induced asthmatic mice revealed significant upregulation of *Adra2a*, which correlated with increased catecholamine metabolism and type 2 inflammation. α2AR was predominantly expressed on follicular helper T (Tfh) cells in germinal centers. Pharmacologic activation of α2AR enhanced Tfh cell differentiation, GC B cell responses, and Akt-S473 phosphorylation, exacerbating asthma severity. Conversely, *Adra2a* deletion in CD4 T cells or inhibition by BRL-44408 reduced Tfh and GC B cell frequencies, serum IgE, and airway inflammation. CD4 T cell-specific *Akt1* knockout mice showed similar reduction in Tfh responses and GC activity. These findings identify α2AR as a novel neuroimmune regulator that amplifies Tfh-GC B axis–driven airway inflammation through Akt signaling, offering a potential therapeutic target for asthma.

Introduction

Bronchial asthma is one of the most common chronic diseases in the world. The total number of asthmatics worldwide has reached more than 300 million, the prevalence of asthma in China is as high as 4.2%, and the incidence of asthma is still increasing overtime[1,2], which has brought a serious disease burden to countries around the world[3–6].

Until now, the pathogenesis of asthma has not been fully elucidated, and immunopathogenesis is one of the most important pathogenic mechanisms of asthma. Available evidence suggests that airway inflammation in asthma is mainly a type 2 immune response[7], involving a variety of immune cells, including Th2 cells[8], eosinophils[9], and IgE-secreting plasma cells[10]. However, it remains to be investigated which factors regulate the development of asthma, and which is the key to achieving individualized and precise asthma treatment.

Researchers have reported the involvement of neuroimmune regulation in the development of asthma disease[11–13]. Sympathetic nerves have a diversity of regulatory effects on asthma, and this diversity results primarily from the action of the neurotransmitters they release on different receptors. Previous studies have shown that β2-adrenergic receptors are expressed on the surface of bronchial smooth muscle cells, and activation of β2-adrenergic receptors results in the diastole of airway smooth muscle cells, relieving symptoms of wheezing and shortness of breath. Norepinephrine can also directly inhibit the secretion of pro-inflammatory factors from immune cells through β2-adrenergic receptors[14]. And recent studies have shown that β2 -adrenergic agonists can directly inhibit ILC2 cells, thereby attenuating IL-33-induced allergic airway inflammation[14,15]. Thus long-acting β2-adrenergic receptor agonists (LABAs) combined with inhaled hormones (ICSs) have been widely used in the treatment of asthma. However, there is still a large number of asthmatic patients suffered from uncontrolled or poorly

controlled symptoms[16,17], and it remains to be explored whether other subtypes of adrenergic receptors, especially α receptors, are involved in the pathophysiologic process of asthma.

The sympathetic nervous system is capable of innervating immune organs throughout the body, directly influencing the immune response and assisting in the maintenance of systemic immune system homeostasis. Sympathetic nerve fibers are distributed in all lymphoid organs (including bone marrow, thymus, spleen, and lymph nodes)[18], and the regulation of immune responses in peripheral tissues by the central nervous system (CNS) is achieved through the release of neurotransmitters, such as catecholamines, which act on adrenergic receptors on the surface of target cells[19,20]. Based on the widespread expression of adrenergic receptors on immune cells[21], both the innate and adaptive immune systems are controlled by signals from the sympathetic nervous system[22–25].

Germinal center reaction (GCR), a collective term for the various events that occur in the germinal center, includes high-frequency mutations in somatic cells, maturation of antibody affinity[26,27], class switching of immunoglobulins[28], and formation of memory B cells[29] and plasma cells[30,31]. In the germinal center response, the interaction between follicular helper T cells and follicular B cells plays an important role. B cells are not only able to present antigens to Tfh cells with their class II molecules and stimulate Tfh cells[32], but also provide co-stimulatory signals to Tfh cells through the expression of ICOSL ligated to ICOS on the surface of Tfh cells[33,34].

Previous studies on the neuro-modulatory mechanisms of asthma have focused more on their bronchoconstrictor and diastolic functions[35,36]; meanwhile, recent studies on neuro-immunity have focused mainly on the role of local neurotransmitters in the airway mucosa on immune cells[37,38]; while sympathetic immune regulation has focused on the adrenergic β-receptors[26]. In this study, we focus on the neural mechanisms regulating the changes in the germinal center (GC) associated with IgE production in bronchial asthma, especially allergic asthma, and we pay special attention to the key sympathetic neurotransmitter, norepinephrine, and specifically to the high-affinity receptor subtype of norepinephrine, α2AR, which is used to modulate the interaction between Tfh and GC B cells through the allergen-norepinephrine-α2AR pathway, thereby affecting IgE production and asthma development. Clarifying the mechanism by which norepinephrine regulates Tfh-GC B interactions and IgE production has the potential to search for potentially novel targets for the treatment of asthma, which is highly innovative and of great clinical value.

We have found that α2AR can participate in the regulation of allergic airway inflammation. In response to allergen stimulation, the synthesis and metabolism of the sympathetic neurotransmitter norepinephrine are increased, and α2AR expression is upregulated in the lungs and draining lymph nodes of the lungs. α2AR is located on follicular helper T cells (Tfh) in lymph node germinal centers of peripheral immune organs. Activation of α2AR increases the level of Akt S473 phosphorylation, promotes Tfh development and activation, drives the germinal center response, contributes to increased differentiation of IgE-

secreting plasma cells, promotes the secretion of the immunoglobulin IgE, and facilitates the release of type 2 inflammatory factors.

Results

Adra2a is upregulated in HDM-induced allergic airway inflammation and is associated with catecholamine metabolism and type 2 inflammation

To establish a mouse model of allergic airway inflammation, C57BL/6 mice were intranasally administered 40 μL of PBS (control) or house dust mite (HDM) extract (0.25 mg/mL) on day 1 and days 6–10. Mice were sacrificed and analyzed on day 14. To explore the involvement of adrenergic receptors in the pathogenesis of HDM-induced airway inflammation, we performed RNA-sequencing on lung tissues from PBS- and HDM-treated mice. Among the differentially expressed genes, *Adra2a* (α2 adrenergic receptor) was significantly upregulated in the HDM group (Fig. 1a) and ranked among the top 30 genes with the most pronounced expression differences (Fig. 1b).

To investigate the relationship between adrenergic signaling, catecholamine metabolism, and type 2 inflammatory responses, we conducted gene set expression comparisons and correlation analyses using the RNA-seq data. The HDM group exhibited significantly higher expression of genes related to catecholamine metabolism and type 2 inflammation (Fig. 1c). Furthermore, *Adra2a* expression positively correlated with key type 2 cytokines and immune-regulatory genes, including *Il4*, *Il13*, *Il33*, *Cxcr5*, *Comt*, and *Cxcl9* (Fig. 1d–e), suggesting a potential role of α2AR in coordinating neuroimmune interactions during allergic airway inflammation.

Adra2a is induced in an IL-33-dependent manner under the stimulation of HDM.

We bred *Il33* KO mice, sensitized and challenged *Il33* KO mice (KOH) with HDM, along with WT mice (WTH) in comparison. Under the stimulation of HDM, *Adra2a* expression was downregulated in KOH mice, compared with WTH mice (Fig. 2.**a**). By bulk RNAseq analysis, we found that *Adra2a* ranked among the top 20 most differentially expressed genes (Fig. 2.**b**). KEGG analysis indicated differential gene enrichment in cytokine-cytokine receptor interaction (Fig. 2.**c**). GO analysis suggested that differential genes were associated with cell chemotaxis and cytokine-mediated responses (Fig. 2.**d**). To investigate the relationship between *Adra2a* expression and inflammatory responses, we analyzed the co-regulation patterns between *Adra2a* and 35 inflammatory markers that were upregulated in HDM-treated mice but downregulated in IL-33 knockout conditions. These markers include chemokines (*Ccl2, Ccl3, Ccl11, Ccl12*, etc.), cytokines (*Il6, Il1b, Il33*), and inflammatory receptors (*Ccr1, Ccr2, Ccr5, Tnfrsf11a*, etc.). *Adra2a* expression showed coordinated regulation with 35 inflammatory markers, demonstrating consistent directional changes across all analyzed inflammatory mediators (Fig. 2e**).** Protein-protein interaction network analysis revealed that *Adra2a* and 35 inflammatory markers form a highly interconnected network (Fig. 2f), constructed using experimentally validated and computationally predicted interactions from the STRING database (version 11.5). These suggested that HDM challenge could induce *Adra2a* expression in an IL-33-dependent manner.

In HDM-induced allergic airway inflammation, α2AR expression in the airways and lymph nodes was upregulated, particularly expressed on Tfh cells within lymph nodes

In HDM-induced allergic airway inflammation, the HE staining indicated a higher degree of inflammation in the lung of HDM-treated mice (Fig. 3.**a, b**). Additionally, the cell and protein levels in the bronchoalveolar lavage fluid (BALF) of the HDM group were significantly higher than those in the PBS group, indicating a higher level of airway inflammation in the HDM group (Fig. 3.**c, d**). Serum IgE levels were tested by ELISA and the expressions of IL-4, IL-5, and IL-13 mRNA in lung tissues were measured by real time-PCR. The results showed that the serum IgE level in HDM mice (Fig. 3.**e**) and the expression levels of IL-4, IL-5 in lung tissues were higher than PBS mice (Fig. 3.**f, g**). Thus, these results proved that the mouse model of HDM-induced allergic airway inflammation was successfully established.

Consistent with our previous results, we verified the increased expression of α2AR in the lung of HDM mice at mRNA and protein level by real time PCR and western blot (Fig. 3.**h-j**). Immunofluorescence staining on pulmonary tissue sections demonstrated the upregulation of α2AR on epithelial cells in HDM mice, compared to the control mice (Fig. 3.**k**). α2AR-positive cells and tyrosine-hydroxylase positive cells demonstrated a close proximity (Fig. 3.**l**). Immunofluorescence showed that α2AR co-localized with Tfh cells and was mainly located in the germinal center of lymphoid follicle. These results suggested that α2AR was predominantly expressed in Tfh cells in lymphoid follicles in mouse mediastinal lymph nodes (Fig. 3.**m**).

In order to further investigate the role of α2AR in asthma pathogenesis, α2AR selective agonist (dexmedetomidine, DEX) and α2AR-selective inhibitor (BRL-44408) were applied. Mice were administrated with DEX and BRL-44408 before HDM challenge. We examined the level of Tfh cells in mediastinal lymph nodes by flow cytometry. The results showed that in the lymph nodes HDM was able to induce a significant increase in the amount of α2AR-positive Tfh cells; DEX treatment combined with HDM stimulation could further elevate the level of α2AR-positive Tfh cells; whereas DEX + BRL-44408 + HDM group showed a decrease in α2AR-positive Tfh level compared to that of the DEX + HDM group (Fig. 3.**n, o**).

HDM challenge enhanced norepinephrine metabolism

Sympathetic neurons release catecholamines, including dopamine, norepinephrine, and epinephrine, which act on dopamine receptors and adrenergic receptors, respectively[18,20]. Catecholamine metabolism originates from the conversion of tyrosine to dopa and dopamine under the action of tyrosine hydroxylase (TH) and dopamine decarboxylase (DDC), followed by the formation of norepinephrine under the action of dopamine hydroxylase (DBH), and then the synthesis of epinephrine under the action of Phenylethanolarnine-N-methyl-transferase (PNMT). Ultimately norepinephrine and epinephrine are converted to a series of metabolites, mainly vanillylmandelic acid (VMA), by the action of monoamine oxidase-A (MAO-A)[39,40].

HDM induced allergic airway inflammation in mice and stimulated α2AR up-regulation, while norepinephrine is indispensable to the activation of α2AR receptors. Thus, we suspected that HDM could promote norepinephrine production and metabolism. The levels of catecholamines and their metabolites in serum were tested by high performance liquid chromatography-tandem mass spectrometry (LC-MS/MS). We found that the serum levels of VMA was significantly higher in HDM-group than in PBS-group mice. Glutathione, 3,4-dihydroxyphenylacetic acid, histidine, 3-hydroxy-o-aminobenzoic acid also showed an up-regulated trend (Fig. 4.**a**). Consistently, the RNA-seq results revealed that VMA was significantly upregulated in the HDM group, while NAS, NME, and Asp were downregulated (Fig. 4.**b, c**). These results showed that HDM challenge can lead to enhanced norepinephrine metabolism.

Adra2a is associated with chemokines and metabolic enzymes of sympathetic neurotransmitters.

According to GSE266438, we analyzed the differential gene expression between non-Tfh and Tfh cells. *Adra2a* expression was significantly higher in Tfh cells than in non-Tfh cells, while chemokines and inflammatory markers were also elevated in Tfh cells (Fig. 5.**a**). Protein interaction network and GO analysis showed that *Adra2a* was associated with chemokines and metabolic enzymes of sympathetic neurotransmitters (Fig. 5.**b-d**).

Adra2a was significantly elevated in GCB-Tfh cells and exhibited positive correlation to catecholamine metabolism pathways and type 2 inflammatory factors

Based on GSE147035, we were able to analyze between non-Tfh, Tfr, Tfh-like, and GCB-Tfh subpopulations. *Adra2a* is significantly elevated in GCB-Tfh cells, compared with non-Tfh, Tfr, Tfh-like cells (Fig. 6a). Consistent with our previous result, *Adra2a* were positively correlated with catecholamine metabolism-related genes and type 2 inflammation-related genes (Fig. 6.**b**). Gene set expression analysis showed that compared to non-Tfh cells, GCB-Tfh cells showed higher expression of catecholamine metabolism genes and significantly higher expression of type 2 inflammatory genes (Fig. 6.**c**). Gene correlation network demonstrated a positive correlation between *Adra2a* and other adrenergic receptors, as well as connections to catecholamine metabolism pathways and type 2 inflammatory factor genes (Fig. 6.**d**).

α2AR activation aggravates allergic airway inflammation and promotes Tfh development.

In order to further investigate the role of adrenergic receptor α2AR in asthma pathogenesis, α2AR receptor-selective agonist (dexmedetomidine, DEX) and α2AR receptor-selective inhibitor (BRL-44408) were applied. Mice were administrated with DEX and BRL-44408 before HDM challenge. To study the role of Tfh cells in the asthma pathogenesis, we examined the level of Tfh cells in mediastinal lymph nodes and spleen by flow cytometry (Gating strategy of Tfh cells, Fig. 7. **a**). The amount of Tfh cells was boosted in DEX + HDM group than those in HDM group. And Tfh level was decreased when treated with BRL-44408 compared to the DEX + HDM group, which was not significantly different from that of the HDM group, however. Besides, all these three groups (HDM, DEX + HDM, DEX + BRL-44408 + HDM) had a higher level of Tfh in the mediastinal lymph node than that of PBS group (Fig. 7.**b**).

We then examined the amount of GC B cells in mouse mediastinal lymph nodes (Gating strategy of GC B cells, Fig. 7.**c**). Similarly, the amount of GC B cells in the mediastinal lymph nodes of mice in the HDM, DEX + HDM, and DEX + BRL-44408 + HDM groups were significantly higher than those in the PBS group. The number of GC B cells in the DEX + HDM group was even more numerous compared to that in the HDM group, whereas under BRL-44408 treatment the level of GC B cell tended to fall back, and there was no significant difference compared with the HDM group (Fig. 7.**d**). These results suggest that α2AR activation can induce GC B cell proliferation in mediastinal lymph node, which plays a potential role in local immunity of the lungs in allergic airway inflammation in asthma.

The expression of type II inflammation cytokines (IL-4, IL-5, IL-13) were tested, and we found that the expression of IL-4, IL-5, and IL-13 was significantly up-regulated in the HDM group, DEX + HDM group, and DEX + BRL-44408 + HDM group compared to the PBS group. Meanwhile, IL-4, IL-5 and IL-13 expression was increased in the lung tissues of mice in the DEX + HDM group compared with the HDM group, while this trend was abrogated by BRL-44408 treatment (Fig. 7.**e-g**), indicating that α2AR activation could promote expression of IL-4, IL-5 and IL-13 in HDM-induced airway inflammation. Consistently, serum IgE level in DEX + HDM mice showed a significant elevation compared with HDM group; whereas DEX + BRL-44408 + HDM mice showed a decrease in IgE level compared with DEX + HDM group (Fig. 7.**h**). We then analyzed α2AR expression between non-Tfh, Tfh, and $CXCR5^+$ cells. Tfh demonstrated a predominant level than non-Tfh and $CXCR5^+$ cells (Fig. 7.**i-j**). In addition, by analyzing GSE147035, we found that GCB-Tfh exhibited the highest level of *Adra2a* among the different T cell subsets (GCB-Tfh, non-Tfh, Tfh-like, Tfr) (Fig. 7.**k**) and positive correlation between *Adra2a* and Tfh development (Fig. 7.**i**). These results demonstrated a critical regulatory role of α2AR in allergic airway inflammation, where α2AR activation exacerbated inflammatory responses, whereas receptor inhibition attenuated disease pathology.

Ablation of Adra2a on $CD4^+$ T cells reduced asthmatic phenotype

We generated $Akt1^{fl/fl}Cd4^{Cre}$ mice, in which the α2AR was knocked out specifically in T cells. The numbers of Tfh cells and GC B cells in the mediastinal lymph nodes of the mice were tested. Under HDM stimulation, the numbers of Tfh and GC B cells in the lymph nodes of $Akt1^{fl/fl}Cd4^{Cre}$ mice were significantly lower than those in WT mice (Fig. 8a-d). We found that compared to WT mice, $Akt1^{fl/fl}Cd4^{Cre}$ mice exhibited reduced edema, hemorrhage, inflammatory cell infiltration, goblet cell hyperplasia, and mucus plugging in the lung after HDM stimulation, leading to a decrease in inflammation scores (Fig. 8e). Type II inflammatory factors and serum IgE level were also reduced in $Akt1^{fl/fl}Cd4^{Cre}$ mice treated with HDM (Fig. 8f-i).

α2AR activation increases amount of IgE B cells and GC B cells

We then examined the amount of IgE^+ B cells and GC B cells in mouse mediastinal lymph nodes (Gating strategy of GC B cells, Fig. 9.**a**). The numbers of IgE^+ B cells and GC B cells in the mediastinal lymph

nodes of mice in the HDM, DEX + HDM, and DEX + BRL-44408 + HDM groups were significantly higher than those in the PBS group. Additionally, the level of IgE^+ B cells and GC B cells in the DEX + HDM group was even more numerous compared to that in the HDM group, whereas under BRL-44408 treatment this trend was abrogated (Fig. 9. **b,c**). These results suggested that α2AR activation can promote GC B cell proliferation and IgE secretion in mediastinal lymph node, which plays a potential role in local immunity of the lungs in allergic airway inflammation in asthma.

Knockdown of Akt1 on $CD4^+$ T cells attenuates α2AR-mediated airway inflammation

Early activation of Tfh cells requires activation of TCR signaling. Activation of the TCR activates the intracellular PI3K-AKT signaling pathway, leading to phosphorylation of the AKT molecule, which positively regulates the activation of T cells[41,42]. To explore the potential role of AKT signaling in asthmatic airway inflammation, we generated *Akt1*$^{fl/fl}$*Cd4*^{Cre} mice, and challenged them with HDM under the pre-treatment with dexmedetomidine. The numbers of Tfh, $pAKT^+$ Tfh, and GC B cells in the mediastinal lymph nodes of *Akt1*$^{fl/fl}$ mice were significantly increased in the case of DEX combined with HDM treatment, whereas this was suppressed in the group of *Akt1*$^{fl/fl}$*Cd4*^{Cre} mice (Fig. 10.**a-g**). At the same time, we observed that the number of Tfh, $pAKT^+$ Tfh, and GC B cells were reduced in *Akt1*$^{fl/fl}$*Cd4*^{Cre} mice compared to *Akt1*$^{fl/fl}$ mice with or without DEX pretreatment (Fig. 10.**a-g**).

We also tested the phosphorylation of AKT molecules under α2AR activation, to figure the role of α2AR in T cell activation and Tfh cell development. Lymph node cells were extracted for *in vitro* culture. The lymph node cells and splenocytes were pre-treated with 100 nM concentration of DEX for 30min before anti-CD3 and anti-CD28 administration. We found that anti-CD3/anti-CD28 antibody could significantly activate the phosphorylation of intracellular AKT-S473, and DEX pretreatment could further up-regulate the AKT signaling pathway in lymph node cells (Fig. 10.**h**). Following HDM stimulation, *Akt1*$^{fl/fl}$*Cd4*^{Cre} mice developed focal inflammatory lesions in the lungs. The extent of these lesions was reduced by treatment with DEX and was also reduced by knockout of *Akt1* in $CD4^+$ cells (Fig. 10.**i**). These findings suggested that α2AR-mediated airway allergic inflammation was dependent on AKT signaling.

Discussion

Although the sympathetic nervous system influences asthma through multiple receptors, research has predominantly focused on the broncho-dilatory effects of β2-adrenergic receptors (β2AR), which are the target of common asthma medications. Our study, however, identified an alternative pathway. In a mouse model of house dust mite (HDM) allergy, we found that allergen challenge led to the upregulation of α2-adrenergic receptors (α2AR). This was accompanied by evidence of enhanced norepinephrine metabolism, including increased dopamine beta-hydroxylase (DBH) expression and elevated vanillylmandelic acid. Together, these results indicated that HDM sensitization triggered a significant increase in norepinephrine production and metabolism, highlighting a potentially important role for the α2AR pathway.

The nervous system plays a critical role in regulating immunoglobulin production and secretion. This is evidenced by the fact that norepinephrine deficiency impairs follicular proliferation and germinal center formation, processes essential for antibody synthesis[43]. To investigate the role of α2-adrenergic receptor (α2AR) signaling in allergic asthma, we pre-treated asthmatic mice with either dexmedetomidine (a selective α2AR agonist) or BRL-44408 (a selective antagonist). Our results demonstrated that α2AR activation with dexmedetomidine promoted IgE secretion, while its inhibition with BRL-44408 reduced IgE levels. This indicated that α2AR signaling was a key regulator of IgE production. We hypothesized that norepinephrine is transported to lymphoid follicles and mediates this effect by acting on α2AR.

Our results localized the α2-adrenergic receptor (α2AR) to T follicular helper (Tfh) cells within germinal centers. Functionally, chemical activation of α2AR promoted the proliferation of both Tfh and germinal center B cells in the pulmonary lymph nodes, enhancing their interaction and modulating the germinal center response to drive the production of IgE-secreting plasma cells. Critically, this effect was localized, as agonist and antagonist treatments had no significant impact on Tfh or GC B cell numbers in the spleen. These findings signified that α2AR played a specific and crucial regulatory role in the local adaptive immune response within the lungs and their draining lymph nodes.

TCR signaling is essential for the early activation of T follicular helper (Tfh) cells. This signaling activates the intracellular PI3K-AKT pathway, resulting in AKT phosphorylation, which is a positive regulator of T cell activation[41]. To investigate the role of α2AR in this process, we cultured lymph node cells and splenocytes *in vitro* and stimulated them with anti-CD3 and anti-CD28 antibodies. We found that chemical activation of α2AR by dexmedetomidine (DEX) further promoted the phosphorylation of AKT at serine 473 (S473) under these T cell-stimulating conditions. Therefore, the α2AR-AKT signaling pathway might represent a promising therapeutic target for asthma.

Our research, while identifying a novel role for α2AR in asthma, also has limitations that point to important future directions. Although we verified that allergic stimulation enhanced catecholamine (norepinephrine and epinephrine) metabolism, the precise mechanism driving this increase has not yet been elucidated. Furthermore, the molecular mechanism by which α2AR signaling directly promoted immunoglobulin class switching to IgE remains incompletely defined. A deeper investigation into these questions will be crucial for a comprehensive understanding of α2AR's function in allergic airway disease.

Our study establishes a novel pathway in which α2-adrenergic receptor (α2AR) signaling exacerbates allergic asthma. Allergen exposure enhances norepinephrine turnover and upregulates α2AR expression in the lungs and draining lymph nodes. We found that α2AR activation on T follicular helper (Tfh) cells could amplify the germinal center response via the Akt-S473 phosphorylation pathway. This promotes the differentiation of GC B cells into IgE-producing plasma cells, elevating IgE levels and aggravating airway inflammation. These findings identify α2AR as a promising target for precise therapeutic interventions in asthma.

Materials and Methods

Animals

Age- and sex-matched 6- to 8-week-old mice were selected to HDM administration. WT C57BL/6 mice were purchased from the Shanghai Laboratory Animal Center. *Adra2a* conditional knock-out mice (*Adra2a*^{flox} mice) were purchased from Shanghai Model Organisms Center, Inc. *Cd4*^{Cre} mice were purchased from Jackson Laboratory (Maine, USA). *Cd4*^{Cre} and *Adra2a*^{flox} mice were crossed to conditionally delete *Adra2a* in CD4^{+} T cells. Mice were bred in specific pathogen-free conditions. All protocols used in this study were approved by the Institutional Animal Care and Use Committee at Shanghai Institute of Immunity and Infection, Chinese Academy of Sciences.

Immunization

C57BL/6 mice received intranasal administration of 40 μL HDM solution (0.25 mg/mL) on day 1 and days 6-10, totaling 10 μg HDM, while control animals received 40 μL PBS on the same schedule. All animals were sacrificed and samples were collected on day 14 of model establishment.

Mouse blood collection

Mice were weighed to calculate appropriate anesthetic dosage and anesthetized via intraperitoneal injection. Following anesthesia, the thoracic cavity was exposed, and blood was slowly collected from the heart using 1 mL syringes pre-rinsed with EDTA. Serum was subsequently isolated by centrifugation.

Bronchoalveolar lavage fluid

Following anesthesia, a ~1 cm incision was made along the ventral midline of the neck. The surrounding tissue was separated to fully expose the trachea. A small incision was made into the trachea, into which a flat-head needle was inserted and ligated. Using a 1 mL syringe, 1 mL of pre-cooled PBS was instilled into the lungs and then aspirated. This instillation and aspiration process was repeated once. The final aspirate was collected and transferred to a 1.5 mL microcentrifuge tube. The sample was then centrifuged at 300 × g for 10 minutes at 4°C.

Lung tissue collection

After exposing chest cavity, remove the heart and its surrounding connective tissue, transect the trachea and collect the lung tissue.

Mediastinal lymph node collection and processing

Mediastinal lymph nodes can be obtained from the back of the trachea. Remove the capsule from the lymph nodes, grind the tissue, and filter through a 70 μm filter to prepare a single-cell suspension.

Spleen collection and processing

Spleen was obtained in the retroperitoneum. Remove the capsule, grind the tissue, filter through a 70 μm filter, lyse the red blood cells to prepare a single-cell suspension.

Flowcytometry

The methods of flow cytometry adhere to the guidelines[21]. Lymph node cells and splenocyte were prepared as described previously. For cell surface staining, cell suspensions were incubated with the antibody cocktails for 30 min at 4 °C. For intracellular cytokine staining, cells were stimulated with Leukocyte Activation Cocktail for 4 h (BD Pharmingen, 550583), which contained 50 ng/ml phorbol12-myristate 13-acetate (PMA), 1 μg/ml ionomycin and 1 μg/ml GolgiPlugTM protein transport inhibitor. Then, Cytofix/Cytoperm Kit (BD Pharmingen, 554714) was used to intracellular cytokines staining. For nuclear protein staining, cells were treated with Transcription Factor Buffer Set (BD Pharmingen, 562574) according to the manufacturer's instructions. Biotin anti-mouse CXCR5, anti-streptavidin-PE, purified anti-mouse CD16/CD32, anti-FVS-BV510, anti-CD4-APC-Cy7, anti-CD44-FITC, anti-CD62L-Percp-cy5.5, anti-PD-1-BV421, anti-CXCR5-PE, anti-ICOS-APC, anti-CD19-APC, anti-GL-7-FITC, anti-FAS-PE-cy7, anti-ICOSL-PE antibodies, anti-IgE-BV421 were used. Flow cytometry experiments were acquired on LSRFortessaTM Flow Cytometer and all data was analyzed in FlowJo (Tree Star, Ashland, OR).

Enzyme-linked immunosorbent assay

The levels of serum IgE were measured with sandwich ELISA kit according to the manufacturer's instructions (BD). Result readings were carried out at a 490 nm wavelength, using a microplate reader (Thermo Scientific).

Western blotting

The lung homogenates and cells were lysed in RIPA buffer (Beyotime) containing protease inhibitor (Bimake). Total protein was measured with Pierce BCA assay and equal amounts of denatured proteins were loaded and run on 10 to 12.5% gradient gel. After transferred to PVDF membranes, the protein was hybridized with indicated primary antibodies and corresponding HRP labeled secondary antibodies. Super ECL Substrate (Tanon, Shanghai, China) was used to detect the bands, which were analyzed and quantitated using Image J software. The primary antibody used in western blot analysis were as follows: Anti-tubulin (11224-1-AP; proteintech); anti-GAPDH (10494-1-AP; proteintech); anti-α2AR antibody (PA1-048; Invitrogen); anti-Akt (pan) antibody (4691T; CST); anti-Phospho Akt (Thr308) antibody (13038T; CST); anti-Phospho Akt (Ser473) antibody (4060T; CST). The original Western blotting gel images are listed in the Supplementary Materials.

Quantitative real-time PCR

Total RNA was extracted from lung homogenates or cultured cells using TRIzol reagent (Invitrogen, Carlsbad, CA) following the manufacturer's instructions. cDNA was generated using a reverse transcriptase kit (FastQuant RT Kit, Tiangen Biotech), followed by quantitative RT-PCR analysis (SYBR Green, TaKaRa). The plate was analyzed on the ABI 7900HT Fast Real-Time PCR System using a 10 μl

reaction volume. The relative expression levels of target genes were determined by the $2^{-\triangle\triangle Ct}$ cycle threshold method. The primers of *Il4, Il5, Il13, Adra2a, Dbh, Maoa* and *Gapdh* were listed as follows:

Mouse Gene	Forward	Reverse
Il4	GGTCTCAACCCCCAGCTAGT	GCCGATGATCTCTCTCAAGTGAT
Il5	GCAATGAGACGATGAGGCTTC	GCCCCTGAAAGATTTCTCCAATG
Il13	CCTGGCTCTTGCTTGCCTT	GGTCTTGTGTGATGTTGCTCA
Adra2a	TCTGGCTGAGAGGGACA	GGGTGTGGAGGAGATAAT
Dbh	GAGGCGGCTTCCATGTACG	TCCAGGGGGATGTGGTAGG
Maoa	GCCCAGTATCACAGGCCAC	CGGGCTTCCAGAACCAAGA
Gapdh	CCCACTAACATCAAATGGGG	CCTTCCACAATGCCAAAGTT

Lung histology

Mouse lung tissues were fixed in 4% formaldehyde overnight at RT. After embedded in paraffin, tissues were cut into 5 μm sections and used for hematoxylin and eosin (HE) and periodic acid-schiff (PAS) staining. Images were taken using CaseViewer software version 3 (DHISTECH, Hungary). The lung inflammation score was determined in a blinded manner, as described previously[44].

RNA-Seq and RNA-Seq data analysis

The wildtype C57BL/6 mice were treated with either PBS or HDM. At designed timepoints, the mice were sacrificed. The lungs were removed and homogenized to extract the total RNA in TRIzol reagent (Invitrogen, Carlsbad, CA). After conducted quantification and qualification, the total RNA of each sample was sequenced using the Illumia platform (Novogene Co., LTD). STRING Database (https://string-db.org) was assessed to analyze the targeted genes which were differentially expressed in our study. GraphPad Prism 8.0.1 (San Diego, CA) was used to analyze difference of genes by Volcano plot.

GEO dataset analysis

We investigated the relationship between α2AR expression and T follicular helper (Tfh) cell development through integrated analysis of publicly available transcriptomic datasets. Gene expression profiles were obtained from GEO datasets GSE266438 and GSE147035, which encompass T cell differentiation states including Tfh cell populations. Statistical analyses were performed using R (version 4.1.0). Differential gene expression analysis was conducted using the limma package with empirical Bayes moderation. Genes with an adjusted p-value < 0.05 and absolute log2 fold change > 1 were considered statistically significant. Protein-protein interaction networks were constructed using STRINGdb (version 11.5) and visualized using igraph and visNetwork packages. Heatmaps were generated using pheatmap with row-wise Z-score normalization and complete linkage hierarchical clustering. Pathway activity scores were

calculated as the mean expression of representative gene sets for adrenergic signaling (*Adra2a, Adrb1, Adrb2*), cytokine response (*Il4, Il33, Il13, Cxcl9*), and catecholamine metabolism (*Th, Ddc, Dbh, Comt*). Correlation analyses were performed using Pearson correlation with pairwise complete observations. All boxplots display median values with interquartile ranges, and statistical comparisons were made using two-sided Student's t-tests with Benjamini-Hochberg correction for multiple comparisons. Data visualization was performed using ggplot2 (version 3.3.5) and related packages.

Metabolic analysis of blood catecholamine and its derivatives

Differential abundance of metabolites between HDM and PBS groups was determined using a two-sided Student's t-test assuming equal variances. Metabolites with a log2 fold change (FC) > 0 and a P-value < 0.05 were considered statistically significant. Multiple testing correction was performed using the Benjamini-Hochberg false discovery rate (FDR) method. Data visualization included a volcano plot highlighting significantly altered metabolites and a heatmap displaying z-score normalized abundance of differentially expressed metabolites, with hierarchical clustering performed using Euclidean distance and complete linkage. All statistical analyses were conducted in R (v4.1.0) utilizing ggplot2 and pheatmap packages.

Correlation Analysis between *Adra2a* and Inflammatory Mediators

To investigate the relationship between *Adra2a* expression and inflammatory responses, we analyzed the co-regulation patterns between *Adra2a* and 35 established inflammatory markers, including chemokines (*Ccl2, Ccl3, Ccl11, Ccl12*, etc.), cytokines (*Il6, Il1b, Il33*), and inflammatory receptors (*Ccr1, Ccr2, Ccr5, Tnfrsf11a*, etc.). Genes showing expression changes in the same direction as Adra2a (log2FC correlation > 0) were classified as co-upregulated or co-downregulated, while those with opposite expression patterns (log2FC correlation < 0) were categorized as inversely regulated. The analysis was restricted to inflammatory markers with detectable expression in our dataset. Visualization was performed using ordered bar plots with *Adra2a*'s fold-change indicated as a reference line, enabling direct comparison of regulatory directionality between *Adra2a* and individual inflammatory mediators across the experimental conditions.

Protein-Protein Interaction Network Analysis

Protein-protein interaction networks were constructed using experimentally validated and computationally predicted interactions from the STRING database (version 11.5) (Figure 2f). The network was visualized using igraph and ggraph packages in R, with the Fruchterman-Reingold algorithm for force-directed layout. Node size was scaled to degree centrality (number of connections), while betweenness centrality (importance in network connectivity) was represented by a blue-green-red color gradient. Edge width and transparency were proportional to STRING combined confidence scores, ranging from low (0.2) to high (2.0) interaction reliability. Node labels were displayed only for proteins above median degree centrality to maintain visual clarity. Network topological parameters were

calculated using standard graph theory metrics, with all visualizations rendered at 300 DPI resolution for publication-quality output.

Statistical data analysis

Statistical analysis of all experimental data was performed in Graphpad Prism 8.0 software. Pooled data were all analyzed for statistical differences by t-test or One wany ANOVA test. The statistical data in the graphs were displayed as mean ± SEM.

Declarations

Acknowledgements

This work is supported by NSFC programs 82170023, 82370025, 82495200/02, 82241042; National Key Research and Development Program of China (No. 2022YFC2304702, 2023YFC2507204, 2024ZD0529805); Innovative Research Team of High-level local Universities in Shanghai (SHSMU-ZDCX20210602); Science and Technology Commission of Shanghai Municipality (20DZ2261200).

Author contributions

G.L.: Study conception and design, data acquisition, analysis and interpretation, and drafting the article. J.D.: Study conception and design, data acquisition, analysis and interpretation. J.C.: Data acquisition, analysis and interpretation. S.X.: Data acquisition, analysis and interpretation. X.L.: Data acquisition, analysis and interpretation. Y.L.: Data analysis and interpretation. C.H.: Data analysis and interpretation. X.D.: Data acquisition. Y.S.: Data acquisition.

G.S.: Study conception and design, analysis, interpretation, and providing funding. X.S.: Study conception and design, data analysis, interpretation, providing funding, drafting and revising the article. All authors read and approved the final manuscript.

Competing interests

All authors declare no competing interests.

References

1. Asher, M. I., García-Marcos, L., Pearce, N. E. & Strachan, D. P. Trends in worldwide asthma prevalence. *Eur Respir J* **56** (2020). https://doi.org/10.1183/13993003.02094-2020
2. Huang, K. *et al.* Prevalence, risk factors, and management of asthma in China: a national cross-sectional study. *Lancet* **394**, 407-418 (2019). https://doi.org/10.1016/s0140-6736(19)31147-x
3. GINA Executive and Science committee. Global strategy for asthma management and prevention: update 2021. 2021.

4. Global, regional, and national deaths, prevalence, disability-adjusted life years, and years lived with disability for chronic obstructive pulmonary disease and asthma, 1990-2015: a systematic analysis for the Global Burden of Disease Study 2015. *Lancet Respir Med* **5**, 691-706 (2017). https://doi.org/10.1016/s2213-2600(17)30293-x
5. Masoli, M., Fabian, D., Holt, S. & Beasley, R. The global burden of asthma: executive summary of the GINA Dissemination Committee report. *Allergy* **59**, 469-478 (2004). https://doi.org/10.1111/j.1398-9995.2004.00526.x
6. Organization WH. Global Health Estimates: Life expectancy and leading causes of death and disability. Published 2019. https://www.who.int/data/gho/data/themes/mortality-and-global-health-estimates.
7. Lötvall, J. *et al.* Asthma endotypes: a new approach to classification of disease entities within the asthma syndrome. *J Allergy Clin Immunol* **127**, 355-360 (2011). https://doi.org/10.1016/j.jaci.2010.11.037
8. Habib, N., Pasha, M. A. & Tang, D. D. Current Understanding of Asthma Pathogenesis and Biomarkers. *Cells* **11** (2022). https://doi.org/10.3390/cells11172764
9. Terl, M. *et al.* Asthma management: A new phenotype-based approach using presence of eosinophilia and allergy. *Allergy* **72**, 1279-1287 (2017). https://doi.org/10.1111/all.13165
10. Matucci, A., Vultaggio, A., Maggi, E. & Kasujee, I. Is IgE or eosinophils the key player in allergic asthma pathogenesis? Are we asking the right question? *Respir Res* **19**, 113 (2018). https://doi.org/10.1186/s12931-018-0813-0
11. Fryer, A. D. *et al.* Neuronal eotaxin and the effects of CCR3 antagonist on airway hyperreactivity and M2 receptor dysfunction. *J Clin Invest* **116**, 228-236 (2006). https://doi.org/10.1172/jci25423
12. Talbot, S. *et al.* Silencing Nociceptor Neurons Reduces Allergic Airway Inflammation. *Neuron* **87**, 341-354 (2015). https://doi.org/10.1016/j.neuron.2015.06.007
13. Nassenstein, C., Krasteva-Christ, G. & Renz, H. New aspects of neuroinflammation and neuroimmune crosstalk in the airways. *J Allergy Clin Immunol* **142**, 1415-1422 (2018). https://doi.org/10.1016/j.jaci.2018.09.011
14. Moriyama, S. *et al.* β(2)-adrenergic receptor-mediated negative regulation of group 2 innate lymphoid cell responses. *Science* **359**, 1056-1061 (2018). https://doi.org/10.1126/science.aan4829
15. Moulton, B. C. & Fryer, A. D. Muscarinic receptor antagonists, from folklore to pharmacology; finding drugs that actually work in asthma and COPD. *Br J Pharmacol* **163**, 44-52 (2011). https://doi.org/10.1111/j.1476-5381.2010.01190.x
16. Kim, L. H. Y., Saleh, C., Whalen-Browne, A., O'Byrne, P. M. & Chu, D. K. Triple vs Dual Inhaler Therapy and Asthma Outcomes in Moderate to Severe Asthma: A Systematic Review and Meta-analysis. *Jama* **325**, 2466-2479 (2021). https://doi.org/10.1001/jama.2021.7872
17. Singh, D. *et al.* Understanding the Clinical Implications of Individual Patient Characteristics and Treatment Choice on the Risk of Exacerbation in Asthma Patients with Moderate-Severe Symptoms. *Adv Ther* **40**, 4606-4625 (2023). https://doi.org/10.1007/s12325-023-02590-2

18. Lubahn, C. L., Lorton, D., Schaller, J. A., Sweeney, S. J. & Bellinger, D. L. Targeting α- and β-Adrenergic Receptors Differentially Shifts Th1, Th2, and Inflammatory Cytokine Profiles in Immune Organs to Attenuate Adjuvant Arthritis. *Front Immunol* **5**, 346 (2014). https://doi.org/10.3389/fimmu.2014.00346
19. Lorton, D. *et al.* Differences in the injury/sprouting response of splenic noradrenergic nerves in Lewis rats with adjuvant-induced arthritis compared with rats treated with 6-hydroxydopamine. *Brain Behav Immun* **23**, 276-285 (2009). https://doi.org/10.1016/j.bbi.2008.10.004
20. Lorton, D., Lubahn, C., Klein, N., Schaller, J. & Bellinger, D. L. Dual role for noradrenergic innervation of lymphoid tissue and arthritic joints in adjuvant-induced arthritis. *Brain Behav Immun* **13**, 315-334 (1999). https://doi.org/10.1006/brbi.1999.0564
21. Chhatar, S. & Lal, G. Role of adrenergic receptor signalling in neuroimmune communication. *Curr Res Immunol* **2**, 202-217 (2021). https://doi.org/10.1016/j.crimmu.2021.11.001
22. Cosentino, M. *et al.* Human CD4+CD25+ regulatory T cells selectively express tyrosine hydroxylase and contain endogenous catecholamines subserving an autocrine/paracrine inhibitory functional loop. *Blood* **109**, 632-642 (2007). https://doi.org/10.1182/blood-2006-01-028423
23. Kenney, M. J. & Ganta, C. K. Autonomic nervous system and immune system interactions. *Compr Physiol* **4**, 1177-1200 (2014). https://doi.org/10.1002/cphy.c130051
24. Elenkov, I. J., Wilder, R. L., Chrousos, G. P. & Vizi, E. S. The sympathetic nerve--an integrative interface between two supersystems: the brain and the immune system. *Pharmacol Rev* **52**, 595-638 (2000).
25. Kohm, A. P. & Sanders, V. M. Norepinephrine and beta 2-adrenergic receptor stimulation regulate CD4+ T and B lymphocyte function in vitro and in vivo. *Pharmacol Rev* **53**, 487-525 (2001).
26. Stohl, L. L. *et al.* Norepinephrine and adenosine-5'-triphosphate synergize in inducing IL-6 production by human dermal microvascular endothelial cells. *Cytokine* **64**, 605-612 (2013). https://doi.org/10.1016/j.cyto.2013.08.005
27. Allen, C. D., Okada, T., Tang, H. L. & Cyster, J. G. Imaging of germinal center selection events during affinity maturation. *Science* **315**, 528-531 (2007). https://doi.org/10.1126/science.1136736
28. Kräutler, N. J. *et al.* Differentiation of germinal center B cells into plasma cells is initiated by high-affinity antigen and completed by Tfh cells. *J Exp Med* **214**, 1259-1267 (2017). https://doi.org/10.1084/jem.20161533
29. Smith, K. G., Weiss, U., Rajewsky, K., Nossal, G. J. & Tarlinton, D. M. Bcl-2 increases memory B cell recruitment but does not perturb selection in germinal centers. *Immunity* **1**, 803-813 (1994). https://doi.org/10.1016/s1074-7613(94)80022-7
30. Huang, C. Germinal Center Reaction. *Adv Exp Med Biol* **1254**, 47-53 (2020). https://doi.org/10.1007/978-981-15-3532-1_4
31. Hägglöf, T. *et al.* Continuous germinal center invasion contributes to the diversity of the immune response. *Cell* **186**, 147-161.e115 (2023). https://doi.org/10.1016/j.cell.2022.11.032
32. Jogdand, G. M., Mohanty, S. & Devadas, S. Regulators of Tfh Cell Differentiation. *Front Immunol* **7**, 520 (2016). https://doi.org/10.3389/fimmu.2016.00520

33. Abdel-Rahman, S. A., Świderek, K. & Gabr, M. T. First-in-class small molecule inhibitors of ICOS/ICOSL interaction as a novel class of immunomodulators. *RSC Med Chem* **14**, 1767-1777 (2023). https://doi.org/10.1039/d3md00150d
34. Liu, D. *et al.* T-B-cell entanglement and ICOSL-driven feed-forward regulation of germinal centre reaction. *Nature* **517**, 214-218 (2015). https://doi.org/10.1038/nature13803
35. Amrani, Y. & Bradding, P. β2-Adrenoceptor Function in Asthma. *Adv Immunol* **136**, 1-28 (2017). https://doi.org/10.1016/bs.ai.2017.06.003
36. Liggett, S. B. The pharmacogenetics of beta2-adrenergic receptors: relevance to asthma. *J Allergy Clin Immunol* **105**, S487-492 (2000). https://doi.org/10.1016/s0091-6749(00)90048-4
37. Steelant, B. *et al.* Histamine and T helper cytokine-driven epithelial barrier dysfunction in allergic rhinitis. *J Allergy Clin Immunol* **141**, 951-963.e958 (2018). https://doi.org/10.1016/j.jaci.2017.08.039
38. Jean, E. E., Good, O., Rico, J. M. I., Rossi, H. L. & Herbert, D. R. Neuroimmune regulatory networks of the airway mucosa in allergic inflammatory disease. *J Leukoc Biol* **111**, 209-221 (2022). https://doi.org/10.1002/jlb.3ru0121-023r
39. Flatmark, T., Almas, B. & Ziegler, M. G. Catecholamine metabolism: an update on key biosynthetic enzymes and vesicular monoamine transporters. *Ann N Y Acad Sci* **971**, 69-75 (2002). https://doi.org/10.1111/j.1749-6632.2002.tb04436.x
40. Tank, A. W. & Lee Wong, D. Peripheral and central effects of circulating catecholamines. *Compr Physiol* **5**, 1-15 (2015). https://doi.org/10.1002/cphy.c140007
41. Sun, Z. *et al.* The kinase PDK1 is critical for promoting T follicular helper cell differentiation. *Elife* **10** (2021). https://doi.org/10.7554/eLife.61406
42. Jutz, S. *et al.* Assessment of costimulation and coinhibition in a triple parameter T cell reporter line: Simultaneous measurement of NF-κB, NFAT and AP-1. *J Immunol Methods* **430**, 10-20 (2016). https://doi.org/10.1016/j.jim.2016.01.007
43. Diniz-Lima, I. *et al.* X-linked immunodeficient (XID) mice exhibit high susceptibility to Cryptococcus gattii infection. *Sci Rep* **11**, 18397 (2021). https://doi.org/10.1038/s41598-021-97041-9
44. Myou, S. *et al.* Blockade of inflammation and airway hyperresponsiveness in immune-sensitized mice by dominant-negative phosphoinositide 3-kinase-TAT. *J Exp Med* **198**, 1573-1582 (2003). https://doi.org/10.1084/jem.20030298

Figures

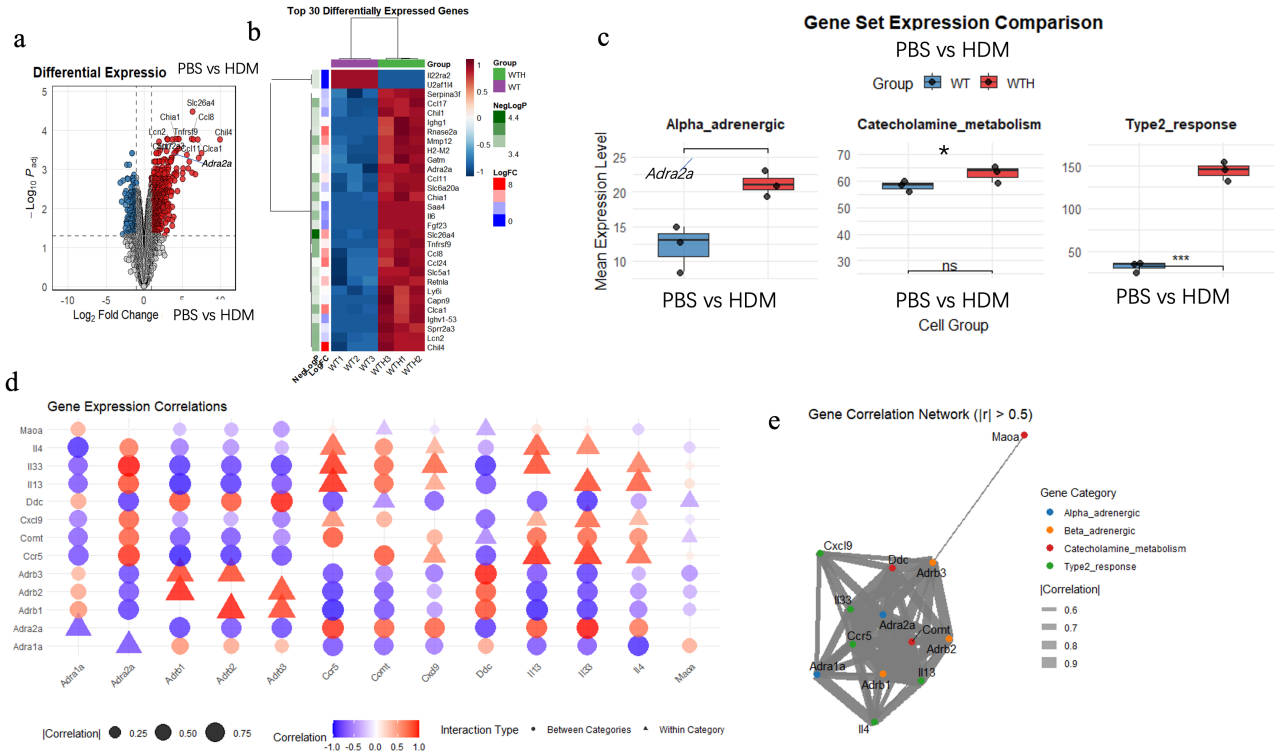


Figure 1

***Adra2a* is upregulated in HDM induced allergic airway inflammation and associated with catecholamine metabolism and type II inflammation. a** Volcano diagram of differential gene expression between PBS and HDM groups. **b** Heat map of top 30 most significantly differentially expressed genes between PBS and HDM groups. **c** Gene set expression comparison indicating significantly higher expression of catecholamine metabolism-related genes and type II inflammation-related genes in the HDM group than in the PBS group. **d** Gene expression correlation analysis showing positive correlations between *Adra2a* and catecholamine metabolism-related genes (*Comt)* and type II inflammation-related genes (*Il4, Il13, Il33, Cxcr5, Cxcl9*). **e** The gene correlation network demonstrating correlations between Adra2a and genes related to catecholamine metabolism and type II inflammation. Data are presented as individual values with mean ± SEM. ns, no significance; *, P < 0.05; **, P < 0.01; ***, P < 0.001.

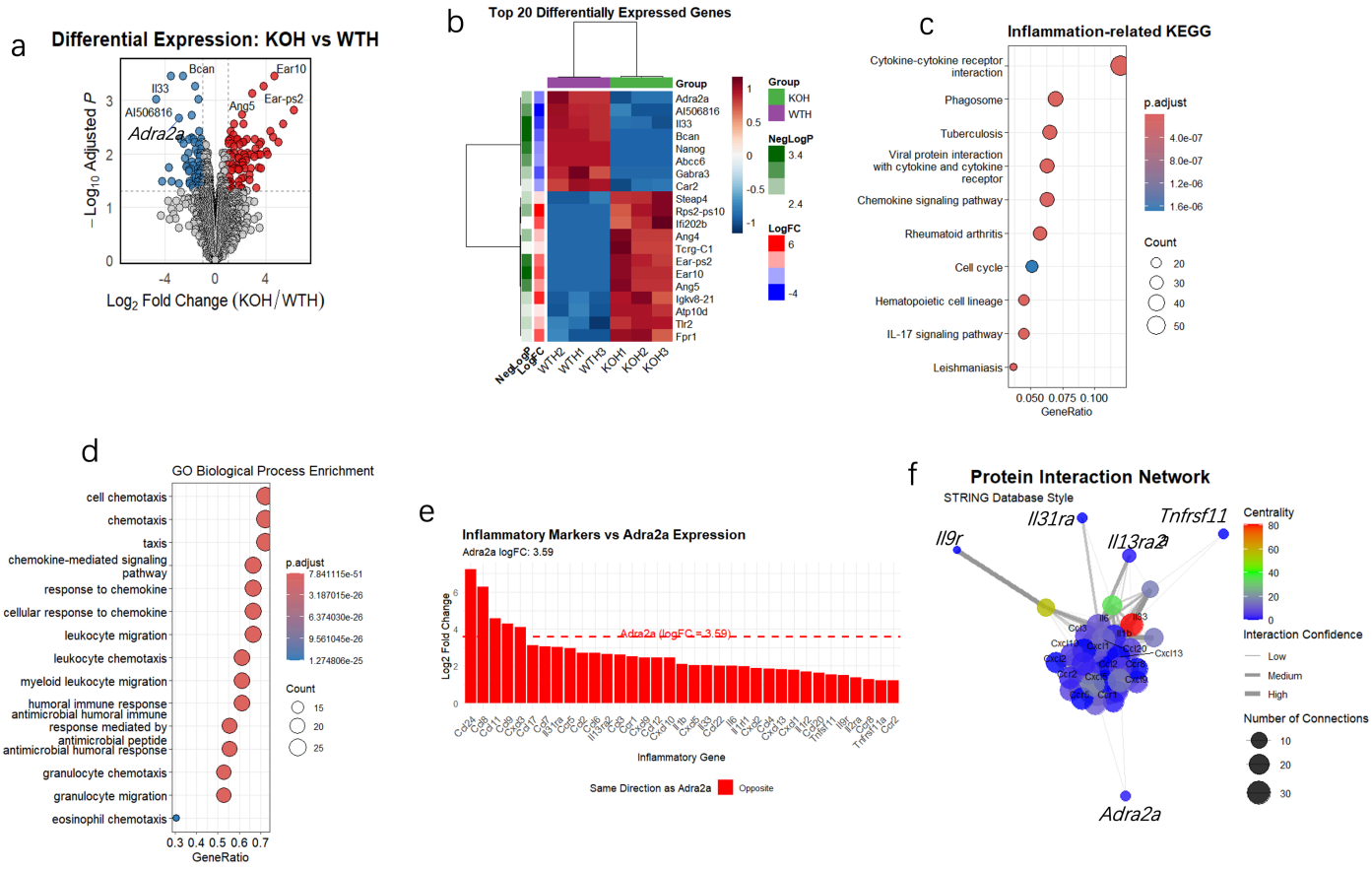


Figure 2

IL-33 knockout mice exhibit downregulated *Adra2a*expression compared to wild-type mice under HDM stimulation, indicating an IL-33-dependent induction of *Adra2a* expression. a Volcano diagram of differential gene expression between KOH and WTH groups. **b** Heat map of top 20 most significantly differentially expressed genes between PBS and HDM groups. *Adra2a*ranked among the top 20 most differentially expressed genes between KOH and WTH groups. **c** Inflammation-related KEGG analysis indicated differential gene enrichment in cytokine-cytokine receptor interaction. **d** GO biological process analysis suggested that differential expressed genes between KOH and WTH groups were associated with cell chemotaxis and cytokine-mediated responses. **e** Analysis of inflammatory markers expression versus *Adra2a*expression (Log2FC=3.59). **f** Protein interaction network analysis indicated a bridging role of *Il33* between inflammatory markers and *Adra2a*.

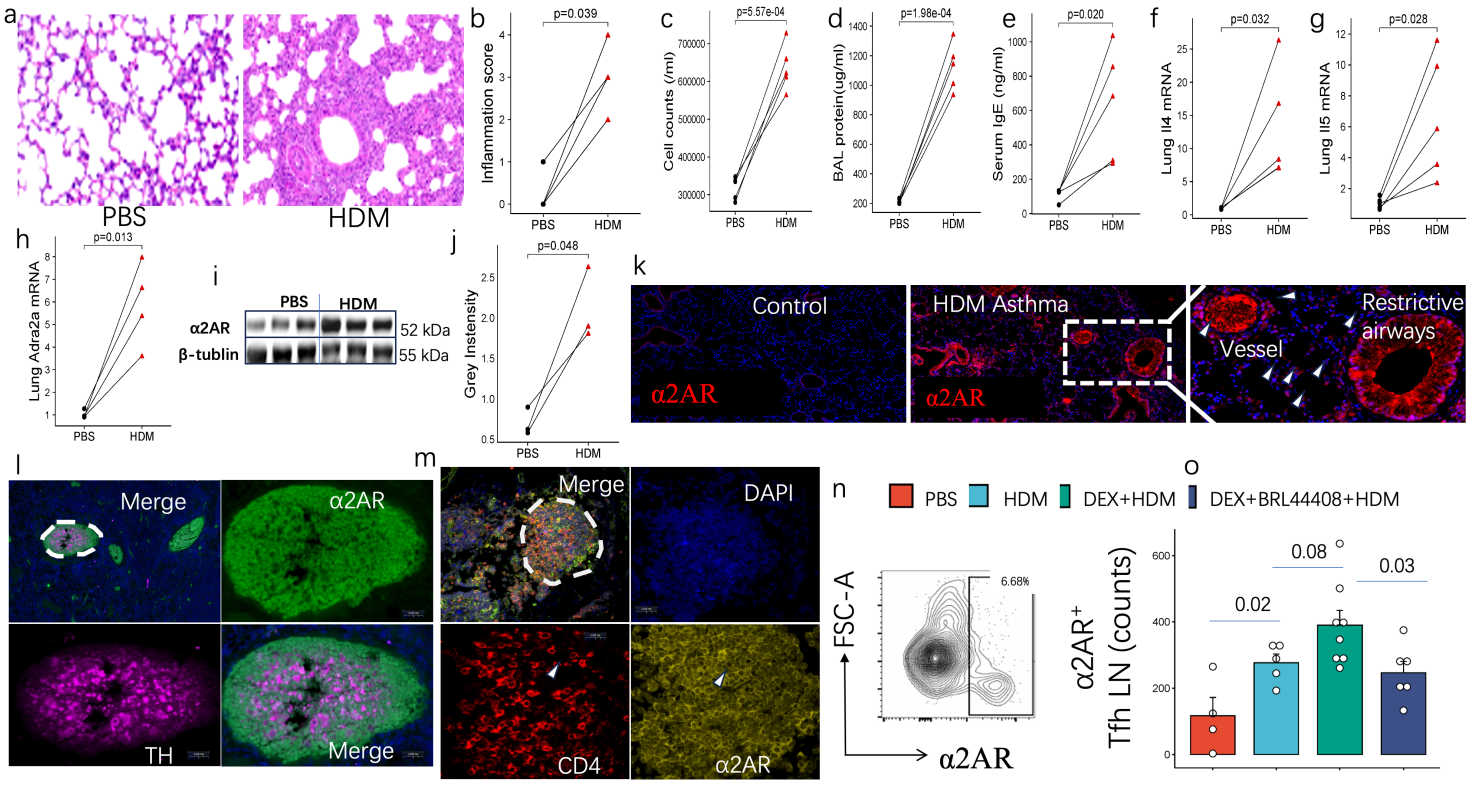


Figure 3

In HDM-induced allergic airway inflammation, *Adra2a* expression in the airways and lymph nodes are upregulated, particularly likely to be expressed on Tfh cells within lymph nodes. a HE staining of lung sections from mice treated with PBS (left) and HDM (right), showing the inflammatory cell infiltration in the lung tissue. HDM-treated mice exhibited higher levels of pulmonary inflammation than PBS-treated mice. **b** Pulmonary inflammation assessments indicated a more severe inflammation in the lung of HDM-treated mice. **c** Total cell number in bronchoalveolar lavage fluid (BALF) from PBS and HDM-treated mice. The HDM group had increased BAL cell counts. **d** Protein concentration in BALF. The HDM group demonstrated elevated BAL protein levels. **e** Serum IgE levels in PBS and HDM-treated mice. The HDM group showed higher serum IgE levels. **f-g** Pulmonary mRNA level of *Il4* and *Il5.* HDM group mice showed significantly higher *Il4* and *Il5* expression in lung. **h-j** Pulmonary mRNA(h) and protein(**i,j**) level of *Adra2a.* HDM group mice showed significantly higher *Adra2a* expression in lung compared to PBS group mice at both mRNA and protein levels. **k** Immunofluorescence staining of lung sections, nuclei were stained with DAPI (blue), α2AR (red). Immunofluorescence indicated α2AR expression on epithelial cells and lymphocytes. **l** Immunofluorescence staining of mediastinal lymph node, showing relationship between $\alpha2AR^+$ and TH^+ cells in mouse lymph nodes (Blue-DAPI; Green-α2AR; Purple-TH). **m** Immunofluorescence staining of mediastinal lymph node, showing relationship between$\alpha2AR^+$ and $CD4^+$ cells in the germinal center of lymph nodes (Blue-DAPI; Yellow-α2AR; Red-CD4). **n** Flow cytometry analysis of $\alpha2AR^+$ Tfh cell in mouse mediastinal lymph nodes. $\alpha2AR^+$ Tfh numbers significantly increased in DEX+HDM mice, with marked reduction upon BRL addition. Data are presented as individual values with mean ± SEM.

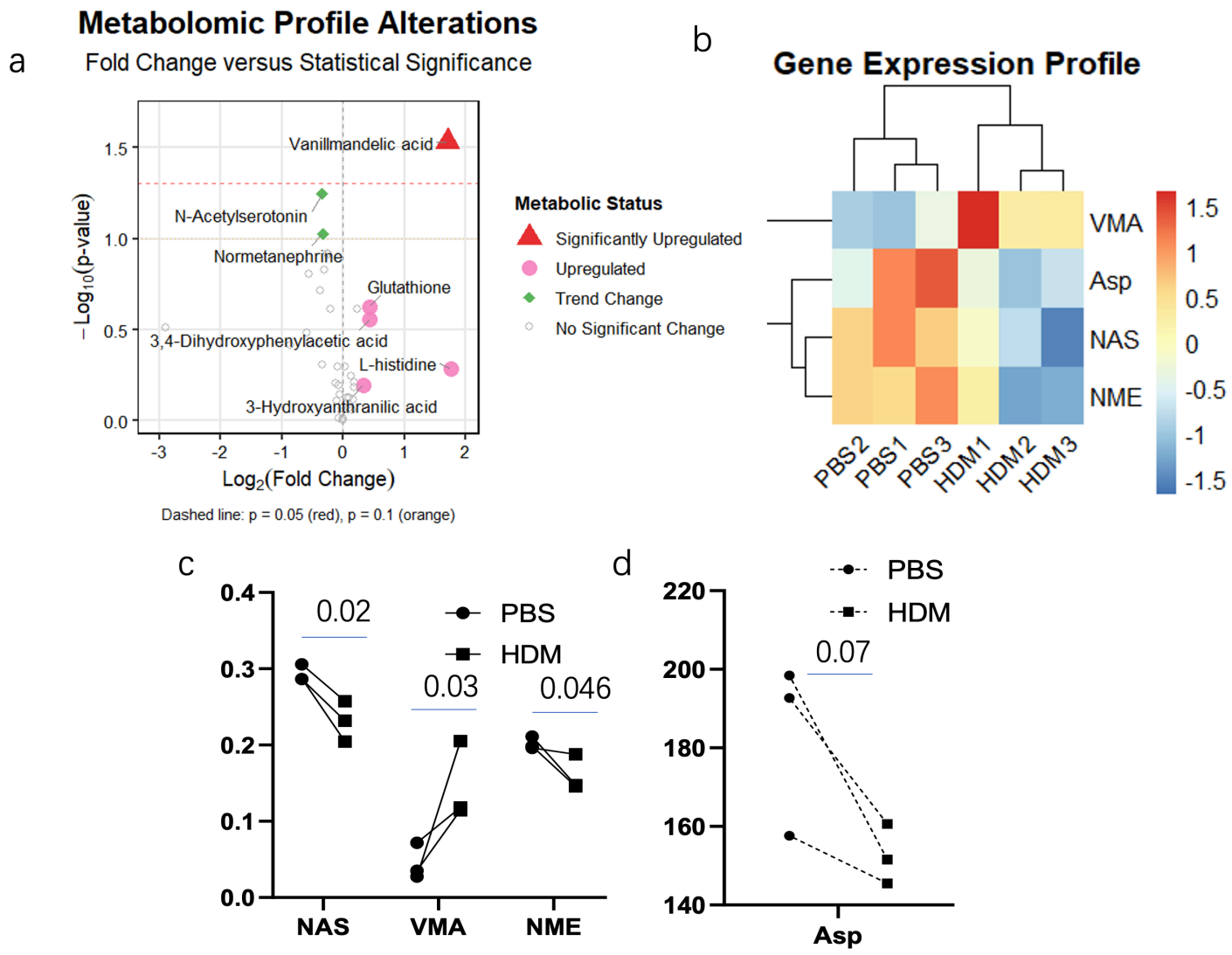


Figure 4

Levels of neurotransmitters and their metabolites in plasma from HDM-group mice and PBS-group mice. a Scatter plot showing the differential expression of catecholamine metabolates in the HDM versus PBS-treated groups. The plot highlights specific proteins that were upregulated. Vanillylmandelic acid, a key metabolite of norepinephrine and epinephrine, was significantly higher in HDM-group mouse plasma than in PBS-group mice. Glutathione, 3,4-dihydroxyphenylacetic acid, histidine, 3-hydroxy-o-aminobenzoic acid, L-histine showed an upward trend. **b** Heat map of VMA, Asp, NAS, NME expression profile in PBS- and HDM-treated mice. **c** NAS and NME were lower in HDM group (P=0.02, 0.046 respectively), whereas VMA higher in the HDM group(P=0.03), indicating enhanced catecholamine metabolism in HDM-treated mice. **d** Asp, an excitatory neurotransmitter, showed a down-regulated trend in HDM group(P=0.07). VMA-Vanillylmandelic acid; NAS-Normetanephrine; NME-Noremetadrenaline; Asp-Aspartic acid.

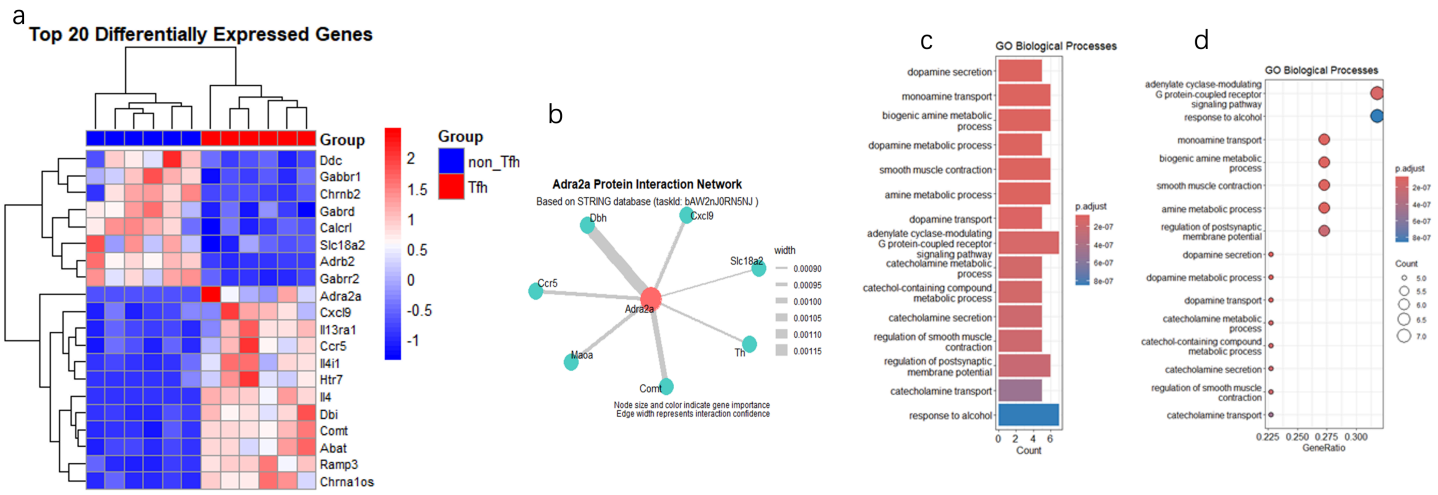


Figure 5

Analysis of *Adra2a* expression on non-Tfh and Tfh cells, based on GSE266438. a Heat map of top 20 differentially expressed genes between non-Tfh and Tfh cells. *Adra2a* expression was significantly higher in Tfh cells than in non-Tfh cells, while chemokines and inflammatory markers were also elevated in Tfh cells. **b** Protein interaction network indicated interaction between Adra2a and metabolic enzymes of sympathetic neurotransmitters, inflammatory chemokines. **c** GO biological process count analysis. **d** GO biological process ratio analysis.

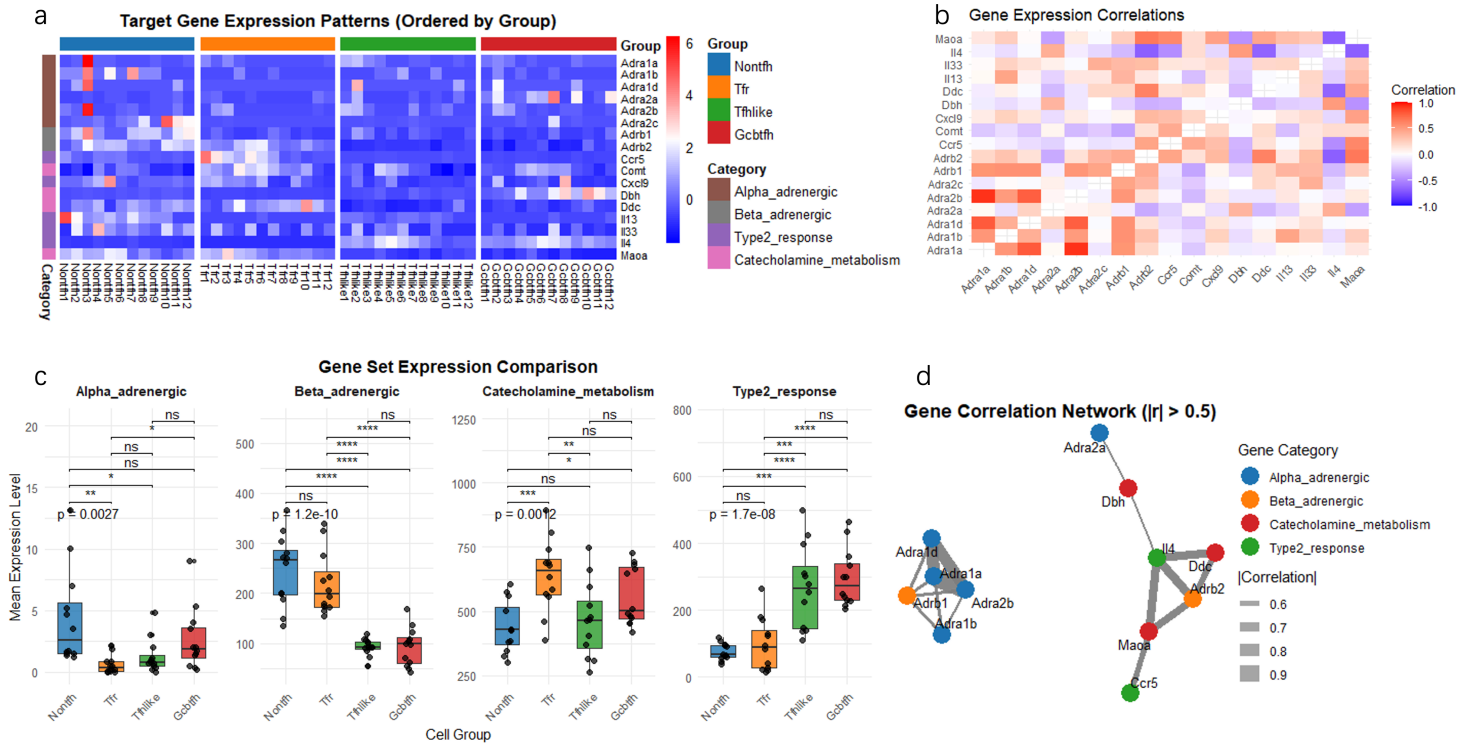


Figure 6

Analysis of non-Tfh, Tfr, Tfh-like, and GCB-Tfh subpopulations. a Target gene expression analysis of non-Tfh, Tfr, Tfh-like, and GCB-Tfh subpopulations. Adra2a was significantly elevated in GCB-Tfh cells. **b** Heat map of gene expression correlation suggested positive correlations between *Adra2a* and catecholamine metabolism-related genes (*Comt*) and type II inflammation-related genes (*Il4, Il13, Il33, Cxcr5, Cxcl9*). **c** Gene set expression analysis showed that compared to GCB-Tfh cells showed higher expression of catecholamine metabolism gene sets and significantly higher expression of type II inflammatory gene sets, non-Tfh cells. **d** Gene correlation network demonstrated relationships between *Adra2a* and other adrenergic receptors, as well as connections to catecholamine metabolism pathways and type II inflammatory factor genes.

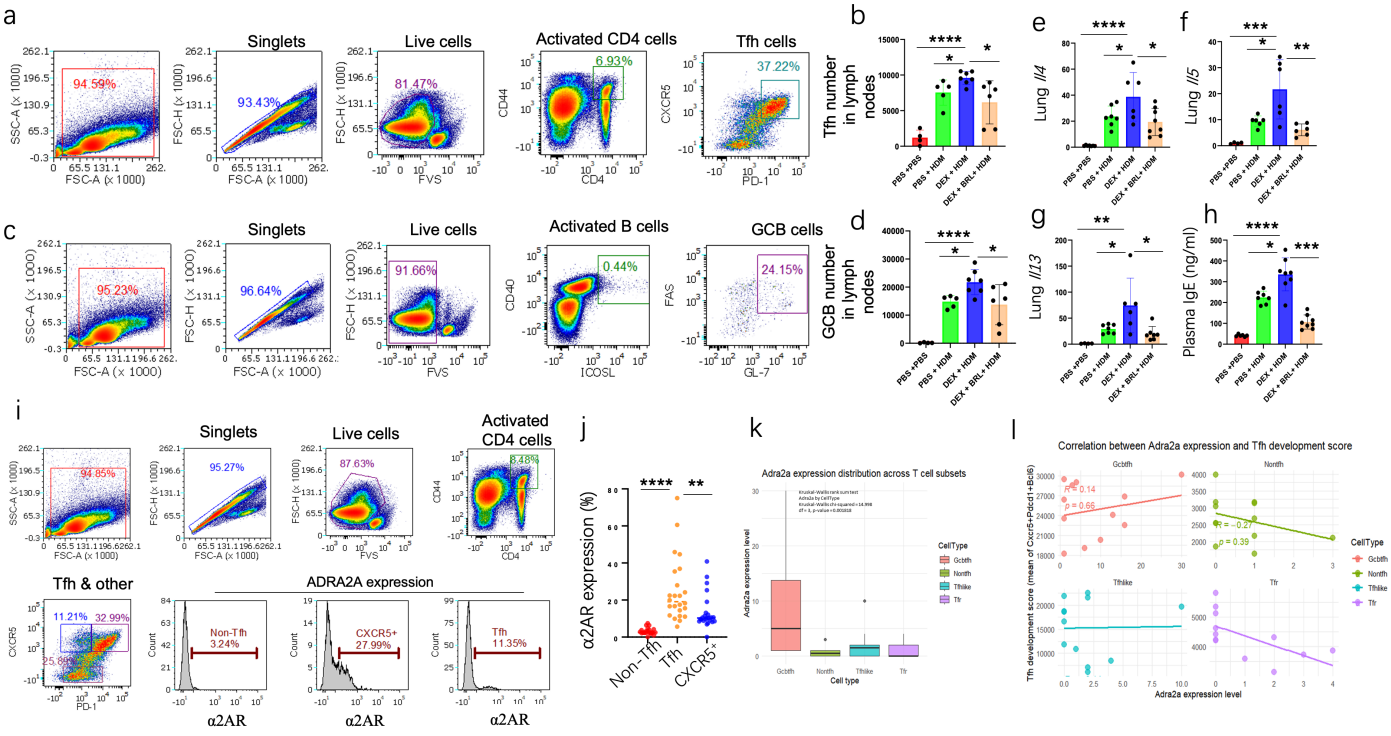


Figure 7

α2AR activation aggravates allergic airway inflammation, and promotes Tfh development. a Gating strategy of Tfh. Tfh cells were marked as $CD4^+CD44^+PD1^+CXCR5^+$ cells. **b** Flow cytometry analysis showed that Tfh levels in DEX+HDM group were higher than PBS+HDM group, and were significantly decreased after BRL addition. **c** Gating strategy of GC B. GC B cells were marked as $CD19^+GL\text{-}7^+FAS^+$ cells. **d** Flow cytometry analysis showed that GC B levels in DEX+HDM group were higher than PBS+HDM group, and were significantly decreased after BRL addition. **e-g** Pulmonary *Il4*, *Il5*, and *Il13* mRNA level of DEX+HDM group mice were significantly higher than in PBS+HDM group, with a marked decrease with BRL administration. **h** Plasma IgE levels in DEX+HDM group mice were significantly higher than in PBS+HDM group, with a marked decrease after BRL administration. **i, j** Flow cytometry analysis of α2AR expression in non-Tfh cells, $CXCR5^+$ cells, and Tfh cells. **k** α2AR expression in different T cell subsets. Tfh cells demonstrated the highest α2AR expression among non-Tfh, $CXCR5^+$ T and Tfh cells. **l**

Relationship analysis of α2AR expression and Tfh development score in different T cell subsets. Data are presented as individual values with mean ± SEM. ns, no significance; *, P < 0.05; **, P < 0.01; ***, P < 0.001; ****, P < 0.0001. DEX: dexmedetomidine, ADRA2a agonist. BRL: BRL-*44408,* ADRA2a antagonist.

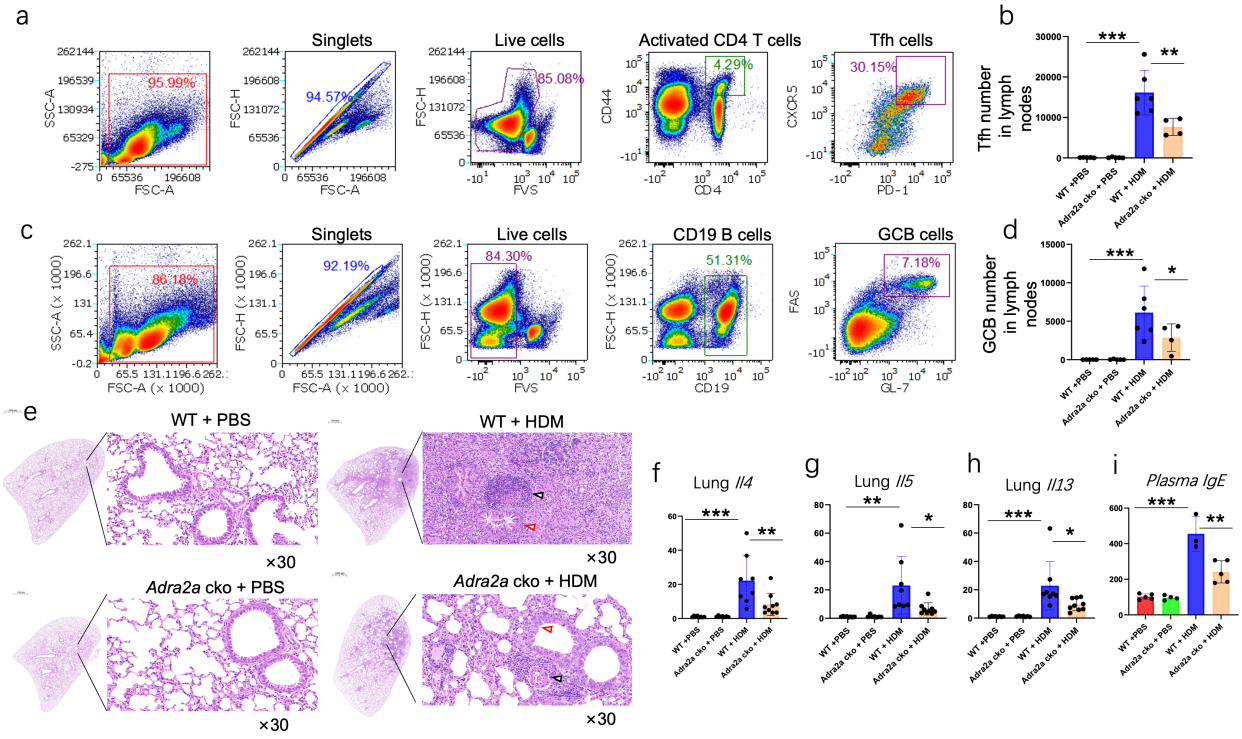


Figure 8

Conditional knockout of *Adra2a* decreases the levels of Tfh and GCB, alleviates inflammation, reduces pulmonary type II inflammatory cytokines, and lowers plasma IgE levels. a Gating strategy of Tfh. Tfh cells were marked as $CD4^+CD44^+PD1^+CXCR5^+$ cells. **b** Flow cytometry analysis showed an obvious reduction in Tfh cells following Adra2a knockout under HDM stimulation. **c** Gating strategy of GC B. GC B cells were marked as $CD19^+GL\text{-}7^+FAS^+$ cells. **d** Flow cytometry analysis showed an obvious reduction in GC B cells following Adra2a knockout under HDM stimulation. **e** HE staining of lung sections demonstrated alleviation of pulmonary inflammation following *Adra2a* knockout under HDM stimulation. **f-h** mRNA analysis showed marked downregulation of pulmonary *Il4*, *Il5*, and *Il13* expression following *Adra2a* knockout under HDM stimulation. **i** Plasma IgE levels were significantly decreased following *Adra2a* knockout under HDM stimulation Data are presented as individual values with mean ± SEM. ns, no significance; *, P < 0.05; **, P < 0.01; ***, P < 0.001.

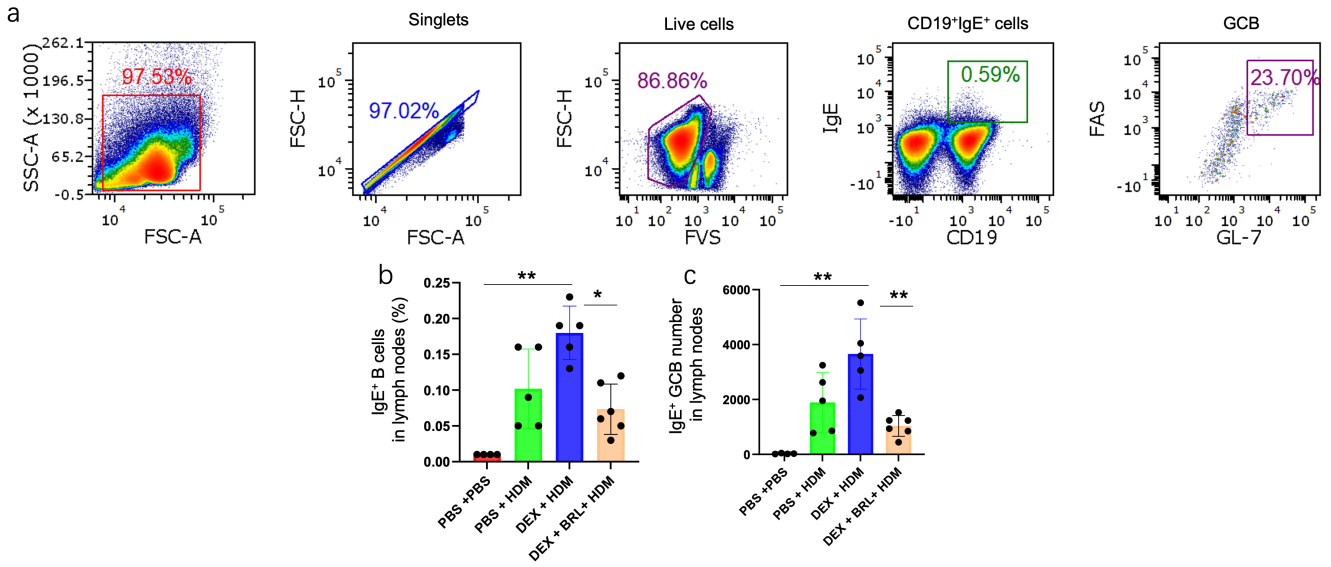


Figure 9

α2AR activation leads to increase amount of IgE⁺ B cells and IgE⁺ GC B cells. a Gating strategy of IgE⁺ B cells and IgE⁺ GC B cells. **b** Ratio of IgE⁺ B cells in the mediastinal lymph nodes. **c** Number of IgE⁺ GC B cells in the mediastinal lymph nodes. Data are presented as individual values with mean ± SEM. ns, no significance; *, P < 0.05; **, P < 0.01; ***, P < 0.001; ****, P < 0.0001.

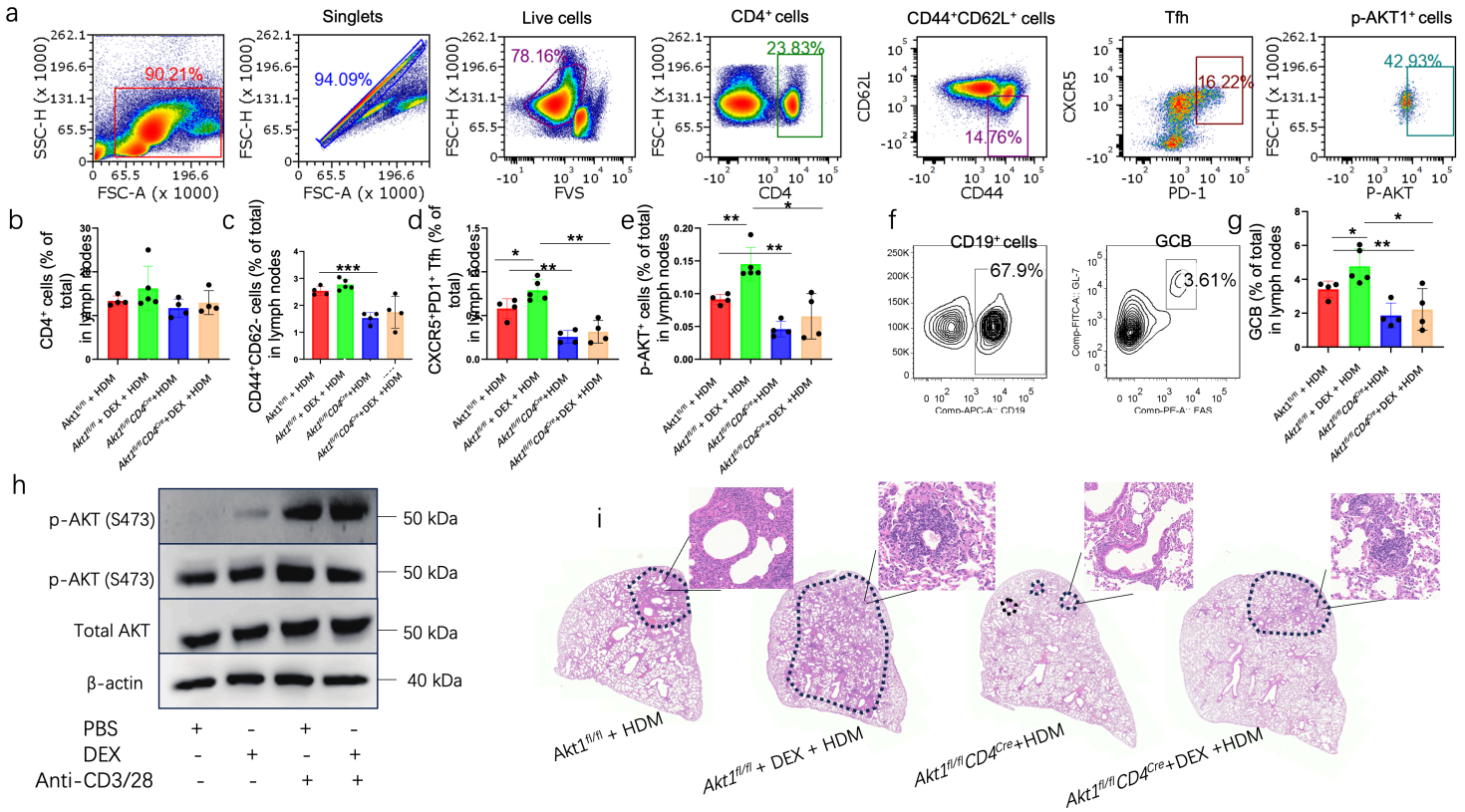


Figure 10

***Akt1* conditional knockout results in a significant attenuation of α2AR-mediated airway inflammation. a** Gating strategy for pAKT$^+$ Tfh cells, marked as CD4$^+$CD44$^+$CD62L$^-$PD1$^+$CXCR5$^+$pAKT$^+$ cells. **b** Flow cytometry analysis of CD4$^+$ cells proportion among *Akt1*$^{fl/fl}$ and *Cd4*^{cre}*Akt1*$^{fl/fl}$ mice with HDM or DEX + HDM treatment. **c** Flow cytometry analysis of CD44$^+$CD62L$^-$ cells proportion among *Akt1*$^{fl/fl}$ and *Cd4*^{cre}*Akt1*$^{fl/fl}$ mice with HDM or DEX + HDM treatment. **d** Flow cytometry analysis of CXCR5$^+$PD1$^+$ cells proportion among *Akt1*$^{fl/fl}$ and *Cd4*^{cre}*Akt1*$^{fl/fl}$ mice with HDM or DEX+HDM treatment. **e** Flow cytometry analysis of p-AKT$^+$ Tfh cells proportion among *Akt1*$^{fl/fl}$ and *Cd4*^{cre}*Akt1*$^{fl/fl}$ mice with HDM or DEX+HDM treatment. **f** Gating strategy of GC B cells, marked as CD19$^+$GL-7$^+$FAS$^+$ cells. **g** Flow cytometry analysis indicated that GCB levels in *Cd4*^{cre}*Akt1*$^{fl/fl}$ mice were significantly lower than in *Akt1*$^{fl/fl}$ mice. **h** Western-blot analysis of AKT phosphorylation, when lymph node cells were isolated, cultured in vitro, and stimulated with DEX combined with CD3/28. Phosphorylation levels of p-AKT at S473 were significantly increased under DEX+CD3/28 trantment. **i** HE staining of lung sections. Following HDM stimulation, *Cd4*^{cre}*Akt1*$^{fl/fl}$ mice developed focal inflammatory lesions in the lungs. However, the extent of inflammatory lesions expanded upon addition of DEX. Data are presented as individual values with mean ± SEM. ns, no significance; *, P < 0.05; **, P < 0.01; ***, P < 0.001.